processes

MDPI

Article

An Optimized Purification Design for Extracting Active ADAMTS13 from Conditioned Media

Katarzyna I. Jankowska [1,†], Upendra Katneni [1,†], Brian C. Lin [1,†], Randilu Amarasinghe [1], Je-Nie Phue [2], Wells W. Wu [2], Nobuko Hamasaki-Katagiri [1], Wojciech Jankowski [1], Rong-Fong Shen [2] and Chava Kimchi-Sarfaty [1,*]

[1] Hemostasis Branch, Division of Plasma Protein Therapeutics, Office of Tissues and Advanced Therapies, Center for Biologics Evaluation & Research, US FDA, Silver Spring, MD 20993, USA; katarzyna.jankowska@fda.hhs.gov (K.I.J.); Upendra.Katneni@fda.hhs.gov (U.K.); Brian.Lin@fda.hhs.gov (B.C.L.); RandiluUmandi.Amarasinghe@fda.hhs.gov (R.A.); Nobuko.Katagiri@fda.hhs.gov (N.H.-K.); wojciech.jankowski@fda.hhs.gov (W.J.)

[2] Facility for Biotechnology Resources, Center for Biologics Evaluation & Research, US FDA, Silver Spring, MD 20993, USA; jenie.phue@fda.hhs.gov (J.-N.P.); wells.wu@fda.hhs.gov (W.W.W.); Rongfong.Shen@fda.hhs.gov (R.-F.S.)

* Correspondence: Chava.Kimchi-Sarfaty@fda.hhs.gov

† These authors contributed equally to this work.

Abstract: ADAMTS13 is a hemostatic enzyme that breaks down pro-thrombotic ultra-large multimers of von Willebrand factor (VWF). The deficiency of ADAMTS13 increases VWF-mediated thrombogenic potential and may lead to thrombotic thrombocytopenic purpura (TTP). Recently, clinical studies have shown the development of acquired TTP after COVID-19 infection and a correlation between low ADAMTS13 plasma levels and increased mortality. As a result, investigating ADAMTS13 as a potential recombinant therapeutic is of broad interest in the field of hematology. ADAMTS13 is considered challenging to purify in its biologically active state. Current purification methods utilize immobilized metal ions, which can interfere with ADAMTS13 metalloprotease activity. For this reason, we optimized an alternative strategy to isolate milligram quantities of highly active recombinant ADAMTS13 (rADAMTS13) from conditioned media after exogenous expression in human cell line, HEK293. HEK293 cells stably expressing C-terminal V5-His-tagged ADAMTS13 were grown in two parallel systems, culture bottles and flasks, for identifying an optimal cultivation strategy. Subsequently, we employed anion exchange followed by anti-V5-tag affinity chromatography to purify rADAMTS13, and extracted rADAMTS13 of high specific activity while preserving its native post-translational modifications. In addition, this process has been optimized and scaled up to produce active rADAMTS13 at levels sufficient for laboratory-scale structural, enzymatic, and biochemical studies.

Keywords: ADAMTS13; purification; V5-tag; von Willebrand factor

Citation: Jankowska, K.I.; Katneni, U.; Lin, B.C.; Amarasinghe, R.; Phue, J.-N.; Wu, W.W.; Hamasaki-Katagiri, N.; Jankowski, W.; Shen, R.-F.; Kimchi-Sarfaty, C. An Optimized Purification Design for Extracting Active ADAMTS13 from Conditioned Media. *Processes* **2022**, *10*, 322. https://doi.org/10.3390/pr10020322

Academic Editor: Florian M. Wurm

Received: 28 December 2021
Accepted: 4 February 2022
Published: 8 February 2022

1. Introduction

ADAMTS13 (A Disintegrin And Metalloproteinase with a ThromboSpondin type 1 motif, member 13) is a metalloprotease enzyme primarily produced and secreted by hepatic stellate cells of the liver and endothelial cells [1–3]. Its primary function is to break down ultra-large multimers of von Willebrand factor (VWF), which are hyperactive in spontaneously agglutinating platelets at sites with damaged endothelium [4–7].

Activity levels of plasma ADAMTS13 vary widely amongst healthy individuals and are assay-dependent. In general, plasmatic ADAMTS13 activity of 40–170% is considered normal for healthy individuals [8]. In addition, it has been demonstrated that the estimated heritability of ADAMTS13 antigen levels is between 59.1% and 83.5% [9]. Any distortion of the ADAMTS13/VWR axis leads to defects in primary hemostasis. Higher ADAMTS13

level (by 35%) has been observed in patients with type 3 von Willebrand disease (VWD) [10]. The absence or decreased activity of ADAMTS13 leads to the persistence of ultra-large VWF multimers (ULVWF) in circulation and may have significant clinical implications (<5% of the activity of a normal pooled plasma). Low ADAMTS13 level has been implicated in thrombosis disorders, such as thrombotic thrombocytopenic purpura (TTP) [11,12]. TTP is thought to be caused by genetic mutations in *ADAMTS13* or acquired etiologies, such as anti-ADAMTS13 autoantibodies, and in the absence of proper treatment, has a high mortality rate of 85–90% [11,13]. Other pathological thrombosis events are also affected by ADAMTS13 deficiency, such as myocardial infarction and ischemic stroke [12,14–18]. In addition, increased clinical attention has been placed on ADAMTS13 recently due to its implications in COVID-19. Clinical studies have revealed that acquired TTP can occur concomitantly with COVID-19 infection, and low ADAMTS13 plasma levels in COVID-19 patients are associated with increased mortality and disease severity [19–21]. For these TTP patients, complement therapy to infuse plasma or plasma-derived product is performed to treat acute TTP episodes. As a potential treatment option to elevate levels of ADAMTS13 in deficient patients, recombinant ADAMTS13 (rADAMTS13) has been under development (ClinicalTrials.gov Identifier: NCT02216084 and NCT03997760) [16,22,23]. Compared to plasma infusion, the use of rADAMTS13 is more efficient and easier to control due to the high concentration and more convenient administration. The use of recombinant proteins offers a significantly lower risk for bloodborne pathogens, allergic reactions, or volume overload [24]. However, further studies are necessary to fully assess the therapeutic applicability, safety, and efficacy of rADAMTS13 as a targeted antithrombotic agent.

While much of the biological characterization of ADAMTS13 has been elucidated, proper assessment of recombinant therapeutic candidates requires a comprehensive investigation of the structure, activity, and immunogenicity of the protein after its production through expression systems and purification. Mature ADAMTS13 (aa #75-1427; active chain) has a complex domain architecture that consists of a catalytic metalloprotease domain, a disintegrin domain, eight thrombospondin type repeat motifs, a cysteine-rich domain, a spacer domain, and two CUB domains [1,4]. The interaction of ADAMTS13 with VWF multimers is mediated through the CUB and spacer domains of ADAMTS13, which undergo slight conformational shifts to support its interaction with VWF [25–28]. Exosites within ADAMTS13 spacer and cysteine-rich domains recognize the A2 domain of VWF, which becomes exposed once elevated shear forces cause VWF to disentangle [25,29]. Subsequently, ADAMTS13 binds VWF via its disintegrin domain, and this interaction facilitates the allosteric activation of the metalloprotease domain to catalyze the breakdown of VWF at the Tyr1605-Met1606 peptide bond within its A2 domain (Figure 1a) [25,27,30–33].

Due to the presence of its disintegrin and catalytic metalloprotease domains, ADAMTS13 is classified as part of the adamalysin family (ADAM and ADAMTS) [34]. This family is further grouped with other metalloproteases, which are enzymes that are appropriately named for their reliance on specific metal ions to facilitate their activities. For the ADAMTS protein family, the catalytic activity of the metalloprotease domain is dependent on interactions with zinc and calcium. The catalytic domain of ADAMTS is conserved, consisting of a zinc-binding motif HEXXHXXGXXH and a methionine domain ("Met-turn"), which structurally supports the zinc catalytic site [35,36]. Due to this proteolytic mechanism, metalloproteases require thorough structural and functional assessments after purification, especially when metals are involved in their isolation. In addition, ADAMTS13 is rich in proline residues, of which 108 of the 118 total prolines reside in its active chain. For large proteins with high numbers of proline residues, protein folding becomes rate-limited by the activity of peptidyl-prolyl *cis-trans* isomerases [37]. Inefficient processing by this enzyme may hinder the accurate folding of ADAMTS13. ADAMTS13 also incurs many post-translational modifications, including *C*-mannosylation, *N*-linked glycosylation, and *O*-fucosylation, which are required for its secretion [38–40]. As a result of its complex structure and unique catalytic mechanism, ADAMTS13 is often regarded as a very difficult protein to isolate in its native and highly active form [41].

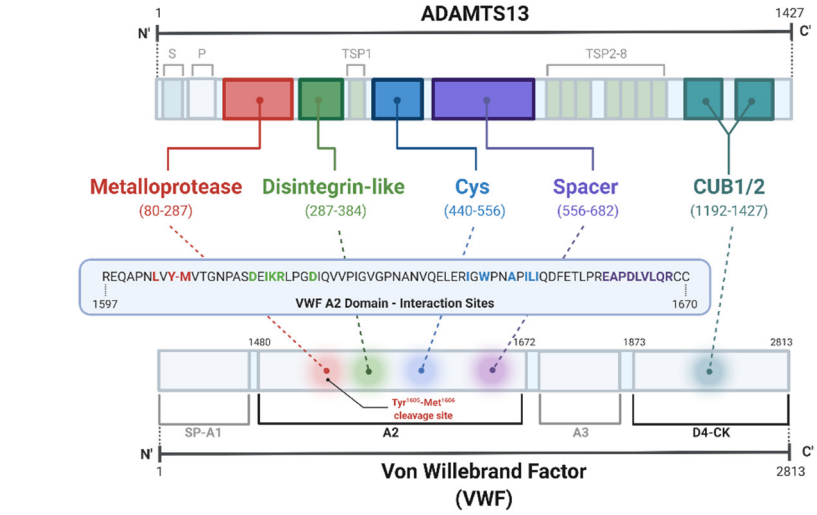

(**a**)

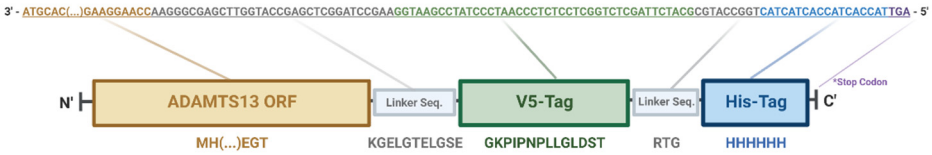

(**b**)

Figure 1. Structure and Domain Interactions of ADAMTS13 with VWF. (**a**) The ADAMTS13 CUB1/2 domains (cyan) bind the D4-CK domains of VWF. This allows ADAMTS13 to form an open conformation, whereby exosites, present within the Disintegrin-like (green), Cys (blue), and Spacer (purple) domains interact with sites within the A2 domain of VWF. Interaction with VWF via the disintegrin-like domain allosterically activates ADAMTS13's metalloprotease domain (red) to cleave VWF at the Tyr1605-Met1606 bond. (**b**) ADAMTS13 construct with V5-His-tag at the C-terminal end with DNA sequences (top) and amino acid sequences (bottom) shown. Created with Biorender.com (accessed on 20 December 2021).

Currently, the most common rADAMTS13 purification schemes rely on nickel affinity chromatography [42,43]. Typical yields from these methods are ~0.1 mg/L due to the low expression of ADAMTS13 [31]. While these purification schemes have been used extensively and are indeed a viable method for purification, there is a need for further optimization. As a metalloprotease, purified ADAMTS13 proteins derived from these purification schemes are not ideal for enzymatic assays as their activity can be influenced by interactions with immobilized metal ions [44–46]. When establishing an optimal purification scheme to extract a protein of interest, it is important to consider factors that may specifically alter the native characteristics of the protein. ADAMTS13 activity, including binding kinetics, can be impacted by factors such as pH and the ionic environment [47,48].

Here, we report an optimized purification design to isolate rADAMTS13 of high activity. We used anion exchange followed by V5-tag affinity chromatography to extract rADAMTS13 from the conditioned media. rADAMTS13 purified through these methods retain its post-translational architecture and has high proteolytic activity. This protocol has been optimized to obtain active tagged rADAMTS13 at large enough quantities for performing laboratory-scale structural and biochemical experiments.

2. Materials and Methods

2.1. Cell Line Generation and Growth

ADAMTS13 (NM_139025.5) and the Flp-In system (ThermoFisher Scientific, Waltham, MA, USA) were used to generate the stable expression cell lines. Unlike lentiviral transfec-

tion systems, the Flp-In system allows for the expression of ADAMTS13 from a single copy integrated at a specified genomic location within the cell line. ADAMTS13 is expressed and secreted into the medium. The *ADAMTS13* sequence was cloned in-frame into the Flp recombination target site vector, pcDN5/FRT/V5-His Topo (ThermoFisher Scientific, Waltham, MA, USA) by GenScript USA Inc. (Piscataway, NJ, USA).

The detailed production of Flp-In HEK293 cells, which stably express C-terminal V5-His-tagged ADAMTS13 under the control of a CMV promoter, was described previously [49]. Briefly, per the manufacturer's instructions, these cells were co-transfected with full-length tagged *ADAMTS13* cDNA cloned into the pcDNA5/FRT vector and pOG44 vector encoding Flp-recombinase enzyme. The selection was performed with 300 µg/mL hygromycin.

The cells were grown and maintained in "serum media", consisting of Dulbecco's Modified Eagle Medium (DMEM) (Quality Biological, Inc., Gaithersburg, MD, USA) supplemented with Pen-Strep, L-glutamine, and 10% fetal bovine serum (Thermo Fisher Scientific, Waltham, MA, USA) and incubated in 5% CO_2 at 37 °C.

2.2. Cell Growth in BelloCell Culture Bottle System

In parallel to culturing in T175 cm^2 flasks, the ADAMTS13-Flp-In HEK293 cell line was grown in the BelloCell system, consisting of 500 mL culture bottles mounted onto a control BelloStage-3000 (Chemglass Life Sciences, Vineland, NJ, USA) and placed in a CO_2 incubator. The bottles were filled with 470 mL of culture media and incubated on stage for 30 min. Meanwhile, the cells, initially grown in 3–4 T75 cm^2 flasks, were collected, counted, and diluted in 30 mL culture media to a concentration of 3.33×10^6 cells/mL. The seeding protocol was followed in accordance with the manufacturer's instructions [50], with cells (100×10^6 cells suspended in 30 mL media) slowly ejected from a sterile pipet onto the matrix with even distribution and cultured with an oscillation rate of 2 mms^{-1} up and down, a top hold time of 20 s, and a down hold time of 0 s. After 4 h, the oscillation speed was reduced to 1 mms^{-1}, with the down holding time of 60 s and the top holding time of 10 s for one bioreactor (A) and 0 s for the second bioreactor (B) to assess two different holding times for proper oxygen transfer from the air to the cells (See Figure 2). Three days after seeding, or when the glucose reading for the media was below 1 g/L, the media was aspirated from the bioreactor and replaced with 500 mL of fresh media. After this, the media was collected and replaced every two days and changed to Opti-MEM reduced serum media (ThermoFisher Scientific, Waltham, MA, USA) after 4 collection cycles (8 days). The cells were cultured in a reduced serum medium for an additional 10 days. During this time, the media was exchanged 5 times, every 48 h (See Figure 3).

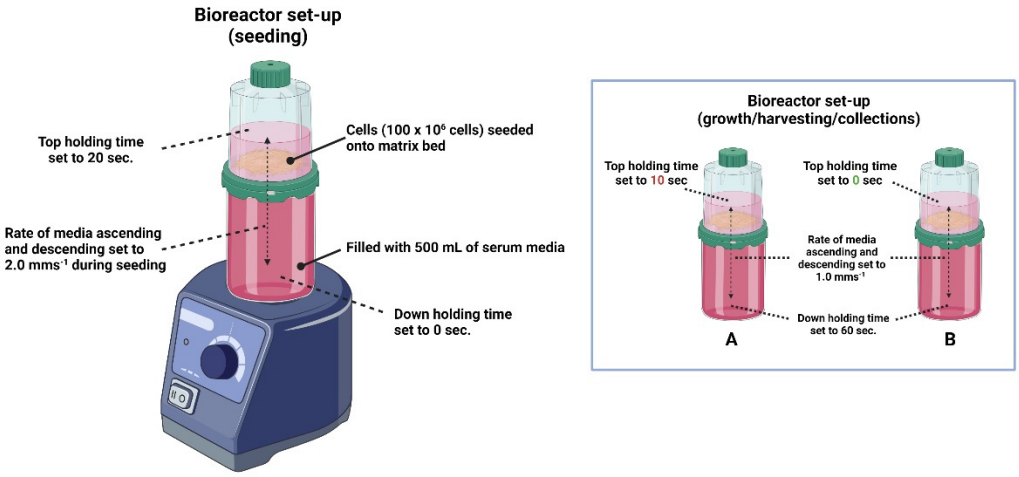

Figure 2. Schematic of bioreactor setup with different top holding times set for bioreactors A and B. Created with Biorender.com (accessed on 20 December 2021).

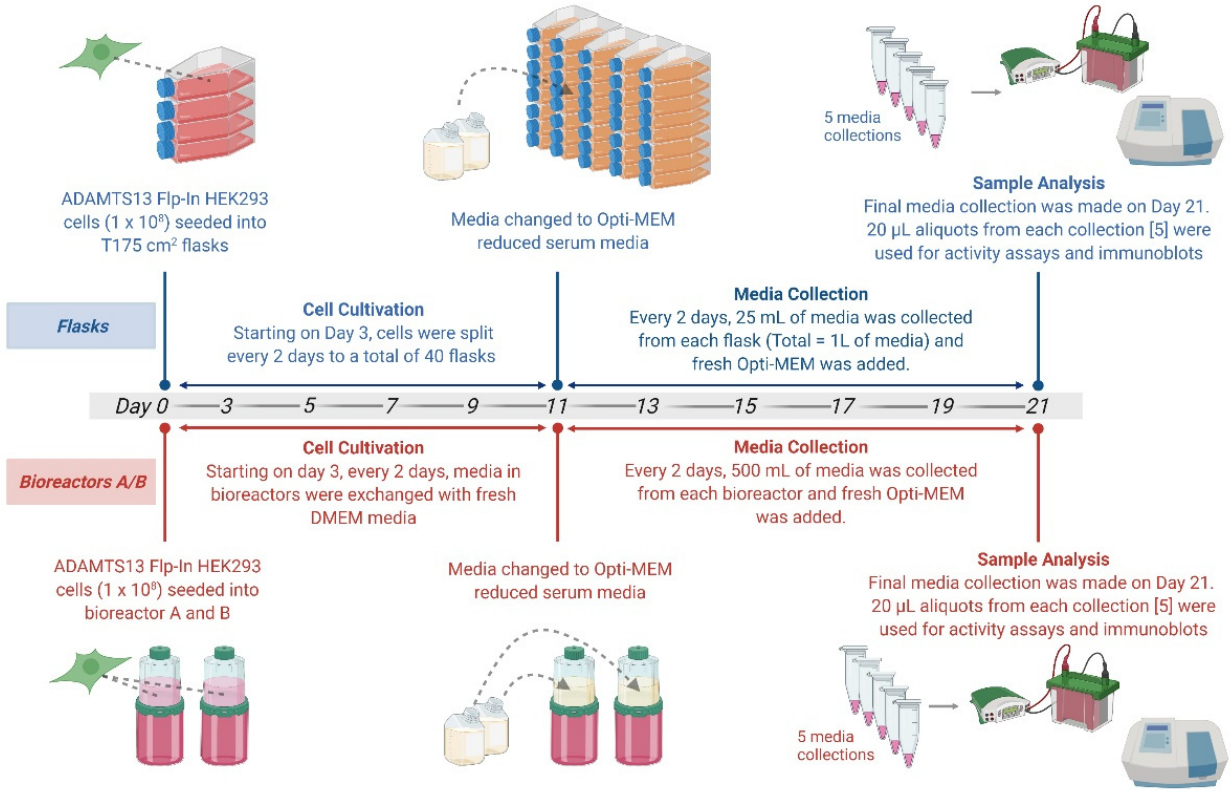

Figure 3. Timeline of bioreactor vs. flask comparison for the cultivation of ADAMTS13 Flp-In HEK293 cells. ADAMTS13 Flp-In HEK293 cells were seeded in parallel within the bioreactor and flask culture systems (1×10^8 cells). At 11 days, media in the flasks were changed to Opti-MEM reduced serum media and were collected every 2 days until day 21. On day 21, the final collection (5th) was made, and the media from each collection was used for activity assay and Western Blot analyses. Created with Biorender.com (accessed on 20 December 2021).

2.3. Cell Harvest and Media Collection

In parallel to the BelloCell culture bottle system, ADAMTS13-Flp-In HEK293 cell lines were grown in T175 cm^2 cell culture flasks under the same cultivation and harvesting timeline as the bioreactors. Cells were seeded at the same density (100×10^6 cells), and were maintained, passaged, and grown to a total of 40 T175 cm^2 flasks by the 11th day of cultivation. After the 11 days of cultivation, the serum media in both culture bottles and flasks were exchanged for Opti-MEM reduced serum media (ThermoFisher Scientific, Waltham, MA, USA). Cells were incubated in this media for 48 h and replaced with fresh reduced serum media after each collection. The media was collected using a vacuum system, filtered through 0.2 µm Nalgene Rapid-Flow vacuum filter units (ThermoFisher Scientific, Waltham, MA, USA). The supernatant was frozen and stored at −80 °C until use.

2.4. rADAMTS13 Purification

For small-scale purification (0.5–2.0 L), the supernatant was concentrated and diafiltrated with 1x PBS buffer using Amicon Ultra-15 (10 kDa) (MilliporeSigma, Burlington, MA, USA) centrifugal filters and rADAMTS13 was purified via V5 affinity purification as described below.

For large-scale purification (4–30 L), the supernatant was first adjusted to pH 8.0 using 2 M Tris-HCl and diluted 3× with de-ionized water prior to Q Sepharose ion-exchange chromatography [31]. To purify the protein from 12 L cell culture supernatant, the diluted supernatant (36 L) was loaded onto 300 mL Q Sepharose Fast Flow resin (Cytiva, Marlborough, MA, USA) packed in an HiScale 50 column (Cytiva, Marlborough, MA, USA) equilibrated with 20 mM Tris-HCl, 50 mM NaCl, pH 8.0 at 4 °C. The column was washed

with the equilibrium buffer until the absorbance at 280 nm returned to base-line, and the protein was eluted with 5 column volumes of 20 mM Tris-HCl, 0.5 M NaCl, pH 8.0. The total elution pool (1.1 L) was concentrated (about 44 times) and diafiltrated with 1x PBS buffer using Amicon Ultra-15 (10 kDa) centrifugal filters. After adding phenylmethylsulfonyl fluoride and benzamidine to the final concentrations of 0.5 and 5 mM, respectively, the total diafiltrated pool (47 mL) was then subsequently purified through V5 affinity purification using anti-V5-tag resin (MBL International Corporation, Woburn, MA, USA) according to the manufacturer's instructions with slight modifications. The pool was applied to a column (2.5 × 20 cm) containing anti-V5-tag resin (7 mL resin per 12 L cell culture supernatant) equilibrated with 1×× PBS buffer, and the column was gently shaken overnight at 4 °C. The column was then washed with 1x PBS buffer, and rADAMTS13 was eluted by V5 peptide (200 µg/mL) in 1× PBS buffer. The elution fractions analyzed by SDS-PAGE were pooled (about 6 fractions), concentrated, and diafiltrated with 1× PBS buffer using Amicon Ultra-15 (10 kDa) centrifugal filters to remove V5 peptides. Protein concentration and yield were determined by Nanodrop 2000C (ThermoFisher Scientific, Waltham, MA, USA). Large-scale protein purification was performed by the Facility for Biotechnology Resources at FDA.

2.5. rADAMTS13 Assessment

2.5.1. Analysis of rADAMTS13 Using SDS-PAGE and Western Blotting

The analysis of rADAMTS13 expression within serum-free media and the purity of the protein was conducted through separation by SDS-PAGE, followed by Coomassie staining (Invitrogen) and/or western blot analysis. Western blots were probed with mouse anti-V5 monoclonal antibody (R960-25, ThermoFisher Scientific, Waltham, MA, USA) paired with a secondary IRDye 800CW goat anti-mouse antibody (LI-COR, Lincoln, NE, USA). The membrane was imaged with a LI-COR Odyssey DLx imaging system (LI-COR, Lincoln, NE, USA). The analysis of band intensities was performed through the LI-COR imaging system analysis tools (LI-COR, Lincoln, NE, USA) and through ImageJ (National Institutes of Health, Bethesda, MD, USA). The representative blot from three individual experiments was analyzed.

2.5.2. rADAMTS13 Antigen Measurement

The quantification of rADAMTS13 in the conditioned media was performed by using the Human ADAMTS13 Quantikine ELISA Kit (R&D Systems, Minneapolis, MN, USA) per the manufacturer's instructions. A standard curve was generated in the range of 50–0.781 ng/mL using human rADAMTS13 standards provided in the kit. Serial dilutions of conditioned media were tested to confirm the proportionality of detected response to dilution. The concentration of rADAMTS13 in the conditioned media samples was determined based on the standard curve, adjusted for dilution, and reported in ng/mL units.

2.5.3. rADAMTS13 Activity Measurement

The activity was measured with FRETS-VWF73 substrate (Vivitide, Gardner, MA, USA) as described previously [44]. The substrate and rADAMTS13 media collected from cultures or purified rADAMTS13 protein were first incubated separately at 37 °C for 5 min. After combining, 60 total fluorescence readings were taken at 1-min intervals by a Victor X3 plate reader (PerkinElmer, Waltham, MA, USA). rADAMTS13 activity was determined as the slope over the first 40 cycles (fluorescence/time). A standard curve was generated from Technozym ELISA ADAMTS13 standards (0–1 IU/mL) and used for conversion of slope to IU. The data were normalized to the volume of samples analyzed (mL). Specific activity (IU/ng) was determined as the activity (IU/mL) divided by the antigen levels (ng/mL), as measured through ELISA assay. Three sets of purified rADAMTS13 and media from culture collections were analyzed. We used an internal unit (IU) to measure ADAMTS13 activity. One internal unit (IU) corresponds to ADAMTS13 activity of 100% for normal pooled plasma (about 1.0 µg/mL) [51].

2.5.4. Glycosylation Analysis

Purified rADAMTS13 proteins (4 µg) in 25 mM ammonium bicarbonate buffer were reduced using DTT (at 56 °C, 30 min), alkylated using iodoacetamide (room temperature in the dark, 30 min), and trypsin-digested overnight. The tryptic peptides were analyzed by nano-LC/MS/MS using Ultimate LC and Fusion Orbitrap MS (ThermoFisher, San Jose, CA), with settings adapted from our previous glyco-proteomic studies [52,53]. Briefly, peptides were first loaded onto a nanotrap (ThermoFisher PepMap C18, 5 µm, 100 Å, 20 mm × 100 µm I.D.), then eluted onto a reversed-phase Easy-Spray column (ThermoFisher PepMap C18, 3 µm, 100Å, 15 cm × 75 µm I.D.) using a linear 120-min gradient of acetonitrile (2–50%) containing 0.1% formic acid at 300 nL/min flow rate. The eluted peptides were sprayed into the Fusion Orbitrap with spray voltage and ion transfer tube temperature set at 1.8 kV and 250 °C, respectively. The data-dependent acquisition (DDA) mode was enabled, and each Fourier Transform (FT) precursor mass MS1 scan (60,000 resolution) was followed by FT DDA-MS2 scans (15,000 resolution) (3-s cycle time). For identifications of *O*-fucosylation and *C*-mannosylation, DDA-MS2 alternated HCD (step collision energy of 20, 30, 40) and EThcD (with ETD supplemental activation with SA collision energy 25). For identifications of N-linked glycosylation, DDA-MS2 HCD (step collision energy of 20, 30, 40) followed with targeted mass trigger (204.0867 and 366.1396 within ±15 ppm mass tolerance and among top 20 abundant ions) to subsequent EThcD (with ETD supplemental activation with SA collision energy 25). Automatic gain control (AGC) targets and maximum injection times were set as "standard" and "auto", respectively.

LC/MS/MS spectra were processed using Byonic software and further analyzed by Byologic software (PMI-Suite 3.8.11, Protein Metrics, Cupertino, CA, USA). Byonic/Byologic search parameters were set according to the parameters employed: tryptic cleavage sites @K/R (fully specific), two mis-cleavage allowed, 25 ppm mass tolerance, common modification of oxidation @M, fixed modification of carbamidomethylation @C, protein database of ATS13_HUMAN, and PEP 2D / Score / Delta Mod Score being ≤0.01, ≥100, ≥10, respectively. For identifications of *O*-fucosylation and *C*-mannosylation, common modification of mannosylation @W was further added, and the glycan database consists of Fuc(1), Fuc(1)Hex(1), HexNAc(1)Hex(1)NeuAc(2), and HexNAc(2)Hex(2)NeuAc(2). For identifications of N-linked glycosylation, the Byonic glycan database of "N-glycan 182 human no multiple fucose.txt" was used.

3. Results

3.1. Purification of rADAMTS13 from Conditioned Media of Flp-In HEK293 Cells

3.1.1. Expression of rADAMTS13 in Flp-In HEK293 Cells

We have previously established a Flp-In HEK293 cell line that stably expresses rADAMTS13 under a CMV promoter with a V5 epitope and 6x histidine-tagged to the C-terminal end of ADAMTS13 separated from the protein sequence by an 11-aa long spacer linker away from metal and binding sites (Figure 1b) [49].

The expression of rADAMTS13 was verified previously by performing western blot analysis on conditioned media from these cells. The blots indicated expression of rADAMTS13, which could be detected through an anti-V5 monoclonal antibody [49]. The same line was used for this study.

3.1.2. Comparison of Flasks and Bioreactors as Optimal Cultivation Strategies

Due to the low expression of rADAMTS13, large quantities of cells are required to extract a useful amount of purified rADAMTS13. To circumvent this scalability issue, we tested two systems in parallel to determine which strategy is optimal for cultivating large quantities of cells. We initially grew the rADAMTS13 stable expression cell line in T175 cm^2 flasks and then seeded these cells into two separate systems at the same seeding density of 100 × 10^6 cells: culture bottles and a set of T175 cm^2 flasks. To further evaluate cellular growth in culture bottles, two sets of bioreactors were assessed, with one culture bottle (A) maintained at a top holding time of 10 s, while the other (B) cultivated at a top holding

time of 0 s to determine which system provides more efficient nutrient and oxygen transfer to the cell (Figure 2).

Proper adaptation of the top holding time has been suggested to improve oxygenation of the system as per the manufacturer's instructions [50]. Advantages to using culture bottles include not only the larger volume and 15,600 cm^2 surface area for cell growth, but also the ability to easily collect multiple large batches of media from the same culture. After 11 days of cultivation in culture media, the cells can expand over 10 times to a density of 3–5 $\times$ 10^9 cells within the matrices of the culture bottle. On the other hand, using large amounts of T175 cm^2 flasks to cultivate cells is a viable technique, but maintaining huge quantities of flasks is cumbersome, and the expansion of cells is limited by the availability of flasks and space within CO_2 incubators. For this comparison study, over the same cultivation period of 11 days, cells grown in flasks were split every 2 days to a total of 40 flasks, while media in the 2 bioreactors were exchanged to fresh culture media on those same days. On the 11th day, the media was exchanged to reduced serum media and the media was collected every 48 h over the course of 10 days (Figure 3).

In comparison of the two parallel systems, media from four to five collections were evaluated for rADAMTS13 antigen and activity levels. Between the two bioreactors, bioreactor A, with a longer top holding time, exhibited a slight increase in antigen and activity levels compared to bioreactor B, suggesting that changing the top holding time of the system from 0 to 10 s may improve the cultivation of Flp-In HEK293 cells (Figure 4). Increasing the top holding time may better supply the cells with nutrients and facilitate the removal of metabolic waste. The first collections from bioreactors A and B yielded rADAMTS13 antigen levels of 140.0 and 122.8 ng/mL and activity of 1.32 and 1.17 IU/mL, respectively. However, unexpectedly, subsequent collections two to five yielded rADAMTS13 of much lower antigen and activity levels (Figure 4c–e). Noticeably, Flp-In HEK293 cells become less adherent when cultivated in reduced serum media over time within the bioreactors. The reduction in the yields of rADAMTS13 (~65–80% decrease) in subsequent collections is likely due to detachment and loss of cells, which occurred 48 h after exchange from the serum media to the reduced serum media. Nevertheless, while we postulate that the loss of cells is responsible for the decrease in yields in subsequent bioreactor collections, the specific activity of bioreactor-derived rADAMTS13 is comparable to that of flasks across all five individual collections (Figure 4e). Further optimization is required for determining optimal conditions for short and long-term cultivation in reduced serum conditions of mildly adherent cells, such as Flp-In HEK293 cells, within the culture bottle system. In contrast to the bioreactor system, the first collection from the flask system yielded an ADAMTS13 antigen level of 223.7 ng/mL and activity of 2.045 IU/mL. Each successive collection produced a small increase in activity and antigen levels of rADAMTS13 compared to the initial collection (Figure 4c–e). These results suggest that using flasks is a viable system for cultivating Flp-In HEK293 cells for long-term growth and harvesting, while the bioreactor system requires additional optimization with a consideration of factors, such as specific cell type adherence characteristics and flow rate within the bioreactor.

3.2. Purification and Quality Assessment of rADAMTS13 from Conditioned Media

During the purification of the low-secreted protein, each extra purification step dramatically reduces the final yield. Thus, for small-scale (0.5–1 L) purification, the conditioned media collected from rADAMTS13-expressing cells was first concentrated on 10 kDa MWCO centrifugal filters and then purified directly via V5 affinity purification. In larger scale (4–30 L) purification, the protein was purified through a two-step process. In the first step, the conditioned media was loaded onto a column with anion exchange resin, Q-sepharose and the bound protein was eluted using 20 mM Tris-HCl, 0.5 M NaCl, and pH 8.0 buffer. After this step, the sample volume was reduced to 25 mL with centrifugation through filter units and dialyzed with 1x PBS. The concentrated elution pool is subsequently purified through a column, packed with V5-resin, and dialyzed with 1x PBS. SDS-PAGE, western blotting, and Coomassie staining revealed a pure extraction of rADAMTS13 with

a band at ~190 kDa (Figure 5a). Most of the rADAMTS13 was eluted in the third to fifth elution fractions.

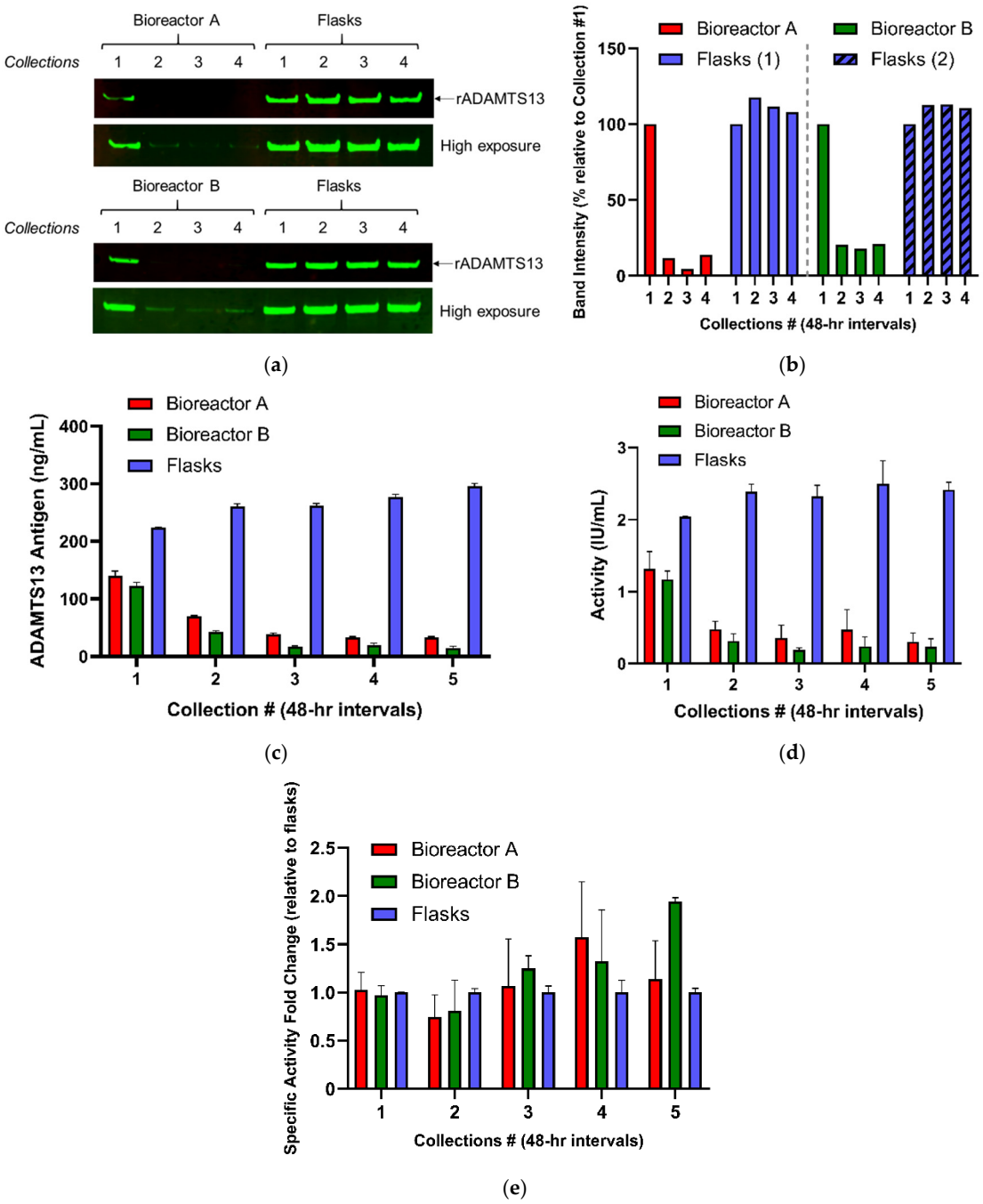

Figure 4. Comparison between bioreactor and flask cultivation systems for rADAMTS13 Flp-In stable HEK293 cells. (**a**) Western blot of V5-tagged rADAMTS13 from collections 1–4, with flask-derived collections shown on the right side adjacent to bioreactor A collections (top) and bioreactor B collections (bottom) for direct comparison; (**b**) Quantification of ADAMTS13 expression shown in western blots in panel A; two groups of flasks are shown for same-blot direct comparison (**c**) rADAMTS13 antigen levels of collections 1–5 from flasks and bioreactors A and B, as measured through ELISA assay; (**d**) Activity of rADAMTS13 in collections 1–5 from flasks and bioreactors A and B, as measured by FRETS-VWF73 activity assay; (**e**) Specific activity of rADAMTS13, as fold changes relative to flasks collections.

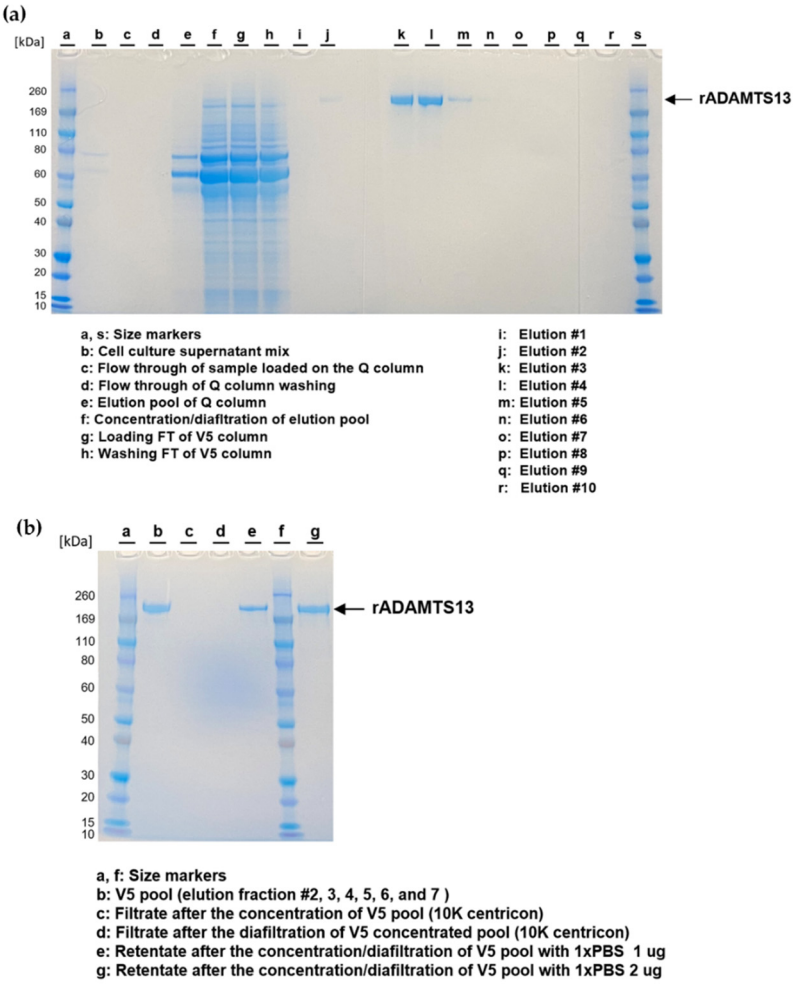

Figure 5. The quality assessment of two-step large-scale purification of V5-tagged rADAMTS13. (**a**) Coomassie staining of representative samples collected at each of the purification steps until the elution of V5-tagged rADAMTS13. (**b**) Coomassie staining of representative samples collected during concentration and diafiltration of the eluted V5-tagged rADAMTS13. The content of all the lanes is mentioned in the figure.

In both cases, the protein yield was comparable or even higher to the yield reported when the protein was purified via His-Tag [31]. In comparison to small-scale purification via only V5-affinity tag or His-Tag purification (yield = 0.10 mg/L of media), the same volume of media from culture bottles purified by QFF followed by V5 provided a yield of 0.145 mg/L, while flask purification produced a yield of 0.678 mg/L (Table 1).

Table 1. rADAMTS13 yields purified from flasks and culture bottles via V5 or QFF + V5.

Purification Method	Flasks (mg/L)	Culture Bottles (mg/L)
His-tag	0.1 [1]	-
V5	0.097	0.113
QFF + V5	0.678	0.145

[1] from reference [31].

Due to the improved long-term cultivation, growth, and harvesting of cells within flasks, purified protein derived from the flask system was used for further protein characterization. To determine the activity of the flask-derived V5-tagged purified rADAMTS13, a FRETS-VWF73 activity assay was performed with purified protein from both small-scale and large-scale purifications (Figure 6).

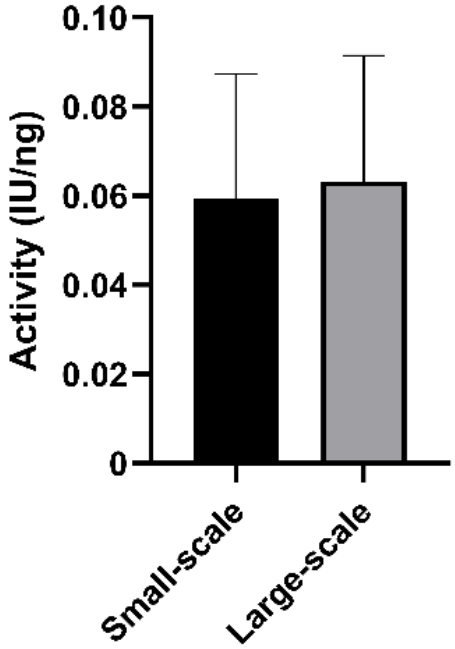

Figure 6. Activity of rADAMTS13 from small-scale V5-affinity purification and two-step large-scale purification, as measured by FRETS-VWF73 activity assay and normalized to the amount of protein analyzed (ng), $n = 3$.

The purified rADAMTS13 showed an activity of 1.37 IU/mL and a specific activity of 0.059 IU/ng from one-step small-scale V5-affinity purification, and purified rADAMTS13 from the two-step large-scale purification yielded ADAMTS13 with an activity of 1.244 IU/mL and a specific activity of 0.063 IU/ng (Table 2).

Table 2. rADAMTS13 protein purified from flasks via V5 or QFF + V5.

Purification Method	Protein Yield (mg/L of Media)	Activity (IU/mL)	Specific Activity (IU/ng)
V5 (small-scale)	0.097	1.366	0.0593
QFF + V5 (large-scale)	0.678	1.244	0.0633

3.3. Post-Translational Modification Analysis of Purified rADAMTS13

Post-translational modifications (PTM) are known to be important for protein expression, folding, and function of a multitude of coagulation factors [4,38,40,54,55]. ADAMTS13 harbors several *N*-glycosylation sites and possesses numerous consensus sites that support *O*-fucosylation and mannosylation modifications, most of which reside in the thrombospondin repeat regions [40,49,56]. Using mass spectrometry, we conducted a glycosylation profile of large-scale, flask-derived purified V5-tagged rADAMTS13 to determine whether the overall PTM architecture of rADAMTS13 is preserved after our two-step large-scale protein purification. We used Byonic software to analyze fragmentation patterns produced through trypsin digestion to determine the presence of core glycan structures and complex individual moieties that are suggestive of *O*-fucosylation and *C*-mannosylation sites.

Glycosylation analysis confirmed that the overall post-translational modification architecture is present in the purified V5-tagged ADAMTS13. Based on our analysis, we were able to identify seven previously reported N-glycosylation sites (Table 3). A few glycosylation sites, N142, N146, and N828, which are present in plasma-derived ADAMTS13, were not detected by this analysis due to low sequence coverage of these regions by trypsin digestion [39,40].

Table 3. *N*-glycosylation data of flask-derived V5-tagged purified rADAMTS13.

Position	Most Abundant Forms	Glycopeptide Assignment of Tryptic Peptides *	Identified Charge States
N552	HexNAc(4)Hex(5)Fuc(1) HexNAc(5)Hex(4)Fuc(1)	CQVCGGDNSTCSPR	+3
N579	HexNAc(5)Hex(3)Fuc(1) HexNAc(5)Hex(4)Fuc(1)	EYVTFLTVTPNLTSVYIANHRPLFTHLAVR	+4 to +6
N614	HexNAc(2)Hex(6)	MSISPNTTYPSLLEDGR	+2 and +3
N667	HexNAc(5)Hex(5)Fuc(1) HexNAc(5)Hex(4)Fuc(1)	YGEEYGNLTRPDITFTYFQPKPR	+4
N707	HexNAc(5)Hex(4)Fuc(1)NeuAc(1)	WVNYSCLDQAR	+3
N1235	HexNAc(6)Hex(3)Fuc(1)NeuAc(1)	VLESSLNCSAGDMLLLWGR	+3
N1354	HexNAc(6)Hex(3)Fuc(1)NeuAc(1)	IAIHALATNMGAGTEGANASYILIR	+4

* All the C's shown are of carbamidomethylated cysteines (using iodoacetamide in alkylation). The *N*-glycosylation sites within tryptic peptides were highlighted with red font.

Furthermore, *O*-fucosylation sites, the majority of which reside in the TSP repeat regions of ADAMTS13, are present in the purified V5-tagged rADAMTS13 (Table 4). In addition, we previously identified an unreported *O*-glycosylation site for ADAMTS13 at the S1170 residue [49]. In this analysis, DiSialyl Core-1 ($NeuAc_2HexHexNAc$) and 2 ($NeuAc_2Hex_2HexNAc_2$) glycans were both identified as forms present at this site, of which the former is more abundant. The W387 residue was identified as a mannosylation site in rADAMTS13, consistent with other studies [39,40].

Table 4. *O*-fucosylation and *C*-mannosylation of flask-derived V5-tagged purified rADAMTS13.

Position	Modification Types	Glycopeptide Assignment of Tryptic Peptides *	Identified Mass †
S399	Fuc(1)Hex(1)	SCGGGVVTR	600.7743 (+2)
S698	Fuc(1)Hex(1)	GPCSVSCGAGLR	764.834 (+2)
S757	Fuc(1)Hex(1)	ELVETVQCQGSQQPPAWPEACVLEPC PPYWAVGDFGPCSASCGGGLR	1378.8608 (+4)
S907	Fuc(1)Hex(1)	TGAQAAHVWTPAAGSCSVSCGR	847.0445 (+3)
S965	Fuc(1)Hex(1)	LAACSVSCGR	694.8052 (+2)
S1027	Fuc(1)Hex(1)	VMSLGPCSASCGLGTAR	1016.4552 (+2)
S1087	Fuc(1)Hex(1)	WHVGTWMECSVSCGDGIQR	858.3629 (+3)
W387	Hex	WSSWGPR	519.2380 (+2)
S1170	HexNAc(1)Hex(1)NeuAc(2) HexNAc(2)Hex(2)NeuAc(2)	GLLFSPAPQPR	1065.4966 (+2)832.3776 (+3)

* All the C's shown are carbamidomethylated cysteines (using iodoacetamide in alkylation). † The identified mass presented in this table is for a peptide with unoxidized M. The *O*-fucosylation and *C*-mannosylation sites within tryptic peptides were highlighted with red font.

Interestingly, in comparison to plasma-derived ADAMTS13, purified V5-tagged rADAMTS13 has a selective preference for different N-linked glycan forms. Most N-linked glycosylation sites in plasma-derived ADAMTS13 are reported to be terminally sialylated [40], but the more abundant N-linked glycans in V5-tagged purified rADAMTS13 are predominantly of the unsialylated forms or contain only one sialic acid. The significance of sialylation on ADAMTS13 is not well understood, but the PTM structure of coagulation factors is highly dependent on a variety of factors, including the PTM machinery of its secreted cell type [55,57]. Nevertheless, though the unsialylated form may be slightly more abundant in purified V5-tagged rADAMTS13, a heterogenous population of sialylated and unsialylated glycan forms were identified at each glycosylation position. Therefore, most importantly, the glycosylation analysis indicates that the majority of previously identified PTM sites are present in V5-tagged purified rADAMTS13 and that the purification process did not alter the post-translational landscape.

4. Discussion

ADAMTS13 is a metalloprotease enzyme, important for degrading ultra-large prothrombotic multimers of VWF to prevent spontaneous agglutination of platelets. For this purpose, ADAMTS13 is regarded as one of the important mediators of hemostasis and a potential target for the development of a recombinant therapeutic for targeting thrombotic disorders. Comprehensive testing must be conducted to evaluate the efficacy, safety, and characteristics of rADAMTS13, which can be performed through laboratory-scale experimentation.

However, to properly assess the structure and function of rADAMTS13, a significant amount of purified rADAMTS13 is required, which has been a challenging task. rADAMTS13 poses many issues for purification due to its relatively large size and low expression in cells. It also undergoes complex post-translational modifications, including extensive glycosylation, and its amino acid sequence is rich in prolines. Furthermore, due to its nature as a metalloprotease by which its catalytic activity is dependent on interactions with metals ions, rADAMTS13 should be ideally purified with methods that exclude potential chelating agents and metal ions, as these may disrupt the proteolytic activity of the protein. For the successful purification of rADAMTS13, these aspects must be carefully factored into the purification scheme and systematically assessed after purification to ensure that rADAMTS13 retains its native structure and function.

Here, we considered these factors and optimized a purification scheme to isolate active rADAMTS13 tagged with both His and V5-epitope to be effectively used in laboratory-scale studies. We discovered that using the V5 epitope for purification resulted in protein of high specific activity. rADAMTS13 protein yield was higher (~0.68 mg/L) than purification through conventional nickel affinity chromatography methods (~0.1 mg/L) [31]. The purity of rADAMTS13 was affirmed through a band at ~190 kDa, identified by SDS-PAGE and Coomassie staining. We postulate that the higher activity may be the result of using non-metals for eluting rADAMTS13. Many metalloproteases have been eluted through nickel affinity chromatography [58,59], but other methods have been designed, which employ alternative chromatography methods that do not rely on metal-ion-affinity purification schemes [60]. Purified metalloprotease proteins derived from these alternative methods may be more suitable if enzymatic analyses are to be performed on these proteins.

We also tested two separate methods for cultivating cells. One was focused on using a BelloCell culture bottle system that could be efficiently and easily managed for batch-harvesting conditioned media for purification. This system, when used at its maximal capacity, provides 15,600 cm^2 surface area for cell growth and has an automated system for supporting a consistent flow rate across the cell matrices. The system provides a powerful tool for achieving high cell density and high productivity but requires further optimizations in serum-free conditions to provide high nutrient and oxygen transfer under minimal shear stress. The other method we tested in parallel was using a flask system, which, when maintained along the same cultivation timeline as the bioreactors, equated to a total surface area of 7000 cm^2. While flasks are known to be great vessels for cultivating cells, at the quantities required for harvesting enough rADAMTS13 for laboratory experiments, flask management becomes difficult and time-consuming. From our analysis, we determined that both methods were viable for harvesting media containing rADAMTS13 of high specific activity. However, media from the bioreactor system yielded approximately ~65–80% less protein in collections 2–4, while a consistently high level of rADAMTS13 expression was maintained through successive flask collections. For cells grown in bioreactors, we used an optimized protocol for protein expression in HEK293 cells cultured in complete media supplemented with FBS [61]. In the absence of FBS, HEK293 cells are very sensitive and easily detached. Thus, we postulate that the decrease in protein expression is largely due to the dissociation of Flp-In HEK293 cells from the bioreactor matrices when cultured over time in reduced serum media. Based on the cell type and its adherence characteristics, the bioreactor system requires adaptations to improve protein yield. We suggest that additional optimization considerations should be implemented, which include increasing the time for

cells to be cultivated in serum and decreasing flow-rate after switching to reduced serum media, especially for harvesting conditioned media from cultures of mildly adherent cells. With these adjustments, cell detachment may be reduced and the yield improved within the bioreactor system. Nevertheless, both systems were able to produce conditioned media containing rADAMTS13 of high specific activity across multiple consecutive collections.

For the purification of conditioned media, we employed and optimized two strategies for purifying V5-tagged rADAMTS13, based on the scale of purification. For small-scale purifications, we used a one-step process to extract rADAMTS13 through V5-affinity purification. This method yielded ~0.13 mg/L of purified rADAMTS13, with an activity of 1.37 IU/mL for flask-derived protein. In comparison, for large-scale purifications with conditioned media of 4–12 L, we optimized a two-step process consisting of flowing media through a QFF system followed by the V5-affinity purification system. With the additional step of the QFF system, the large-scale purification provided a yield of 0.67 mg/L from flask-derived media and with an activity of 1.24 IU/mL. Regardless of the purification method, the activity of rADAMTS13 is within a normal range (above 1 IU) [8]. The significant increase in purification yield in large-scale purification suggests that the addition of the QFF step substantially improves the protein quality and quantity. In fact, we observed that when a centrifugal filter was used to concentrate the cell supernatant in small-scale purification, the viscosity of the sample also increased due to the presence of the serum and other components of cell culture media. As a result, its downstream processing and scale-up were difficult. In addition, the specific components of the medium that remained in the sample could also be affecting the purification process, the activity, and other properties of the protein. The QFF column, which allowed us to remove phenol red, the serum, and other media components and, at the same time, concentrates the sample and exchanges the buffer solution. We chose the QFF column as it was also previously used for ADAMTS13 purification via His-tag [31], but it is possible that another ion exchange column would be equally effective.

We further verified that post-translational modifications were retained in the flask-derived purified V5-tagged rADAMTS13. We found that seven well-known N-glycosylation sites are present in our purified V5-tagged rADAMTS13 protein, and most of the fucosylation and mannosylation sites, identified in previous studies [40], were preserved as well. Furthermore, our construct does not include a proteolytic cleavage site. The removal of the V5 tag would require an additional purification step, and this would cause the additional loss of purified protein. Since the purified protein maintains its activity in the presence of the additional linker, we decided that the removal of the V5 tag is not critical. To remove the V5 and His-tags by proteases, the spacer linker would have to be modified to include a proteolytic cleavage site motif. Within the ADAMTS13 construct, an enzyme recognition site can be introduced between the open reading frame of rADAMTS13 and the tag sequence for standard enzymatic removal of the tagged element. This technique has been effectively implemented to remove various types of affinity tags from proteins of interest [62]. In some cases, the removal of the tag may be beneficial or critical, as it will prevent any potential interference of the tag with analytical assays.

Furthermore, ADAMTS13 expression level in mammalian cell culture systems is very low. While there are various methods that can be used to achieve higher expression rates, including through codon or codon pair optimization, which is frequently used in the production of recombinant proteins [63,64] or changing the cell type to one with a more efficient system, such as CHO cells [65,66], our priority was to preserve the native gene sequence, protein structure and function, and to express the protein in human cell lines. Here, we have optimized the expression and purification of ADAMTS13 using a similar cellular system to those previously used for the purification of ADAMTS13 via His-tagged methods [31]. Nevertheless, it would be interesting to learn if some suspension cells, such as serum-free cell lines derived from HEK293 (specifically Expi293 or PER.C6) or other highly tranfectable cell systems, would further improve the ADAMTS13 expression yield.

Moreover, we chose stable over transient expression via the Flp-In vector to gain the advantage of a highly controlled expression system for ADAMTS13. We assessed a series of culturing conditions for HEK293 cells and performed protein purification using different strategies to achieve the highest expression efficiency. We demonstrated that even ADAMTS13, a low-expressing protein, may be produced at high yields when culture conditions are well optimized. In combination with protein purification via QFF and V5-affinity columns, we were able to obtain a protein yield almost seven times higher than previously reported purification systems [31]. Therefore, the QFF and V5 affinity purification system provides an optimal means to produce large yields of rADAMTS13 of high purity and activity. This system may be beneficially adapted for the purification of other metalloproteases that may be deleteriously affected by standard metal ion affinity purification methods.

Author Contributions: Conceptualization, K.I.J., U.K., B.C.L., N.H.-K., W.J. and C.K.-S.; methodology, K.I.J., U.K., B.C.L., R.A., J.-N.P., N.H.-K. and W.J.; formal analysis, K.I.J., U.K., B.C.L., R.A., J.-N.P. and W.W.W.; investigation, K.I.J., U.K., B.C.L., R.A., J.-N.P. and W.W.W.; resources, R.-F.S. and C.K.-S.; data curation, K.I.J., U.K., B.C.L. and R.A.; writing—original draft preparation, K.I.J., U.K., B.C.L., N.H.-K. and C.K.-S.; writing—review and editing, K.I.J., U.K., B.C.L., R.A., J.-N.P., W.W.W., N.H.-K., W.J., R.-F.S. and C.K.-S.; supervision, R.-F.S. and C.K.-S.; funding acquisition, C.K.-S. All authors have read and agreed to the published version of the manuscript.

Funding: This research was funded by CBER operating funds.

Institutional Review Board Statement: Not applicable.

Informed Consent Statement: Not applicable.

Data Availability Statement: All data are available and presented within this article.

Acknowledgments: We would like to acknowledge Long Zheng, University of Kansas Medical Center for fruitful discussions.

Conflicts of Interest: The authors declare no conflict of interest.

Disclaimer: Our comments/contributions are an informal communication and represent our own best judgments. These comments do not bind or obligate the FDA.

References

1. Shang, D.; Zheng, X.W.; Niiya, M.; Zheng, X.L. Apical sorting of ADAMTS13 in vascular endothelial cells and Madin-Darby canine kidney cells depends on the CUB domains and their association with lipid rafts. *Blood* **2006**, *108*, 2207–2215. [CrossRef] [PubMed]
2. Pickens, B.; Mao, Y.; Li, D.; Siegel, D.L.; Poncz, M.; Cines, D.B.; Zheng, X.L. Platelet-delivered ADAMTS13 inhibits arterial thrombosis and prevents thrombotic thrombocytopenic purpura in murine models. *Blood J. Am. Soc. Hematol.* **2015**, *125*, 3326–3334. [CrossRef] [PubMed]
3. Zhou, W.; Inada, M.; Lee, T.-P.; Benten, D.; Lyubsky, S.; Bouhassira, E.E.; Gupta, S.; Tsai, H.-M. ADAMTS13 is expressed in hepatic stellate cells. *Lab. Investig.* **2005**, *85*, 780–788. [CrossRef]
4. Zheng, X.L. Structure-function and regulation of ADAMTS-13 protease. *J. Thromb. Haemost.* **2013**, *11* (Suppl. 1), 11–23. [CrossRef] [PubMed]
5. Ruggeri, Z.M. Von Willebrand factor, platelets and endothelial cell interactions. *J. Thromb. Haemost.* **2003**, *1*, 1335–1342. [CrossRef]
6. Barg, A.; Ossig, R.; Goerge, T.; Schneider, M.F.; Schillers, H.; Oberleithner, H.; Schneider, S.W. Soluble plasma-derived von Willebrand factor assembles to a haemostatically active filamentous network. *Thromb. Haemost.* **2007**, *97*, 514–526. [CrossRef]
7. Furlan, M. Von Willebrand factor: Molecular size and functional activity. *Ann. Hematol.* **1996**, *72*, 341–348. [CrossRef]
8. Mannucci, P.M.; Canciani, M.T.; Forza, I.; Lussana, F.; Lattuada, A.; Rossi, E. Changes in health and disease of the metalloprotease that cleaves von Willebrand factor. *Blood* **2001**, *98*, 2730–2735. [CrossRef]
9. Ma, Q.; Jacobi, P.M.; Emmer, B.T.; Kretz, C.A.; Ozel, A.B.; McGee, B.; Kimchi-Sarfaty, C.; Ginsburg, D.; Li, J.Z.; Desch, K.C. Genetic variants in ADAMTS13 as well as smoking are major determinants of plasma ADAMTS13 levels. *Blood Adv.* **2017**, *1*, 1037–1046. [CrossRef]
10. Mannucci, P.M.; Capoferri, C.; Canciani, M.T. Plasma levels of von Willebrand factor regulate ADAMTS-13, its major cleaving protease. *Br. J. Haematol.* **2004**, *126*, 213–218. [CrossRef]
11. Page, E.E.; Kremer Hovinga, J.A.; Terrell, D.R.; Vesely, S.K.; George, J.N. Thrombotic thrombocytopenic purpura: Diagnostic criteria, clinical features, and long-term outcomes from 1995 through 2015. *Blood Adv.* **2017**, *1*, 590–600. [CrossRef] [PubMed]

12. Zheng, X.L. ADAMTS13 and von Willebrand factor in thrombotic thrombocytopenic purpura. *Annu. Rev. Med.* **2015**, *66*, 211–225. [CrossRef] [PubMed]
13. Saha, M.; McDaniel, J.K.; Zheng, X.L. Thrombotic thrombocytopenic purpura: Pathogenesis, diagnosis and potential novel therapeutics. *J. Thromb. Haemost.* **2017**, *15*, 1889–1900. [CrossRef] [PubMed]
14. Lambers, M.; Goldenberg, N.A.; Kenet, G.; Kirkham, F.J.; Manner, D.; Bernard, T.; Mesters, R.M.; Junker, R.; Stoll, M.; Nowak-Göttl, U. Role of reduced ADAMTS13 in arterial ischemic stroke: A Pediatric Cohort Study. *Ann. Neurol.* **2013**, *73*, 58–64. [CrossRef] [PubMed]
15. Xu, H.; Cao, Y.; Yang, X.; Cai, P.; Kang, L.; Zhu, X.; Luo, H.; Lu, L.; Wei, L.; Bai, X.; et al. ADAMTS13 controls vascular remodeling by modifying VWF reactivity during stroke recovery. *Blood* **2017**, *130*, 11–22. [CrossRef]
16. Eerenberg, E.S.; Teunissen, P.F.; van den Born, B.J.; Meijers, J.C.; Hollander, M.R.; Jansen, M.; Tijssen, R.; Beliën, J.A.; van de Ven, P.M.; Aly, M.F.; et al. The role of ADAMTS13 in acute myocardial infarction: Cause or consequence? *Cardiovasc. Res.* **2016**, *111*, 194–203. [CrossRef]
17. Chion, C.K.N.K.; Doggen, C.J.M.; Crawley, J.T.B.; Lane, D.A.; Rosendaal, F.R. ADAMTS13 and von Willebrand factor and the risk of myocardial infarction in men. *Blood* **2006**, *109*, 1998–2000. [CrossRef]
18. Katneni, U.K.; Ibla, J.C.; Hunt, R.; Schiller, T.; Kimchi-Sarfaty, C. von Willebrand factor/ADAMTS-13 interactions at birth: Implications for thrombosis in the neonatal period. *J. Thromb. Haemost.* **2019**, *17*, 429–440. [CrossRef]
19. Mancini, I.; Baronciani, L.; Artoni, A.; Colpani, P.; Biganzoli, M.; Cozzi, G.; Novembrino, C.; Boscolo Anzoletti, M.; De Zan, V.; Pagliari, M.T.; et al. The ADAMTS13-von Willebrand factor axis in COVID-19 patients. *J. Thromb. Haemost.* **2021**, *19*, 513–521. [CrossRef]
20. Tang, N.; Li, D.; Wang, X.; Sun, Z. Abnormal coagulation parameters are associated with poor prognosis in patients with novel coronavirus pneumonia. *J. Thromb. Haemost.* **2020**, *18*, 844–847. [CrossRef]
21. Hindilerden, F.; Yonal-Hindilerden, I.; Akar, E.; Kart-Yasar, K. COVID-19 associated autoimmune thrombotic thrombocytopenic purpura: Report of a case. *Thromb. Res.* **2020**, *195*, 136–138. [CrossRef] [PubMed]
22. Scully, M.; Knöbl, P.; Kentouche, K.; Rice, L.; Windyga, J.; Schneppenheim, R.; Hovinga, J.A.K.; Kajiwara, M.; Fujimura, Y.; Maggiore, C.; et al. Recombinant ADAMTS-13: First-in-human pharmacokinetics and safety in congenital thrombotic thrombocytopenic purpura. *Blood* **2017**, *130*, 2055–2063. [CrossRef] [PubMed]
23. Turecek, P.L.; Peck, R.C.; Rangarajan, S.; Reilly-Stitt, C.; Laffan, M.A.; Kazmi, R.; James, I.; Dushianthan, A.; Schrenk, G.; Gritsch, H.; et al. Recombinant ADAMTS13 reduces abnormally up-regulated von Willebrand factor in plasma from patients with severe COVID-19. *Thromb. Res.* **2021**, *201*, 100–112. [CrossRef] [PubMed]
24. Franchini, M. Plasma-derived versus recombinant Factor VIII concentrates for the treatment of haemophilia A: Recombinant is better. *Blood Transfus.* **2010**, *8*, 292–296. [CrossRef]
25. Petri, A.; Kim, H.J.; Xu, Y.; de Groot, R.; Li, C.; Vandenbulcke, A.; Vanhoorelbeke, K.; Emsley, J.; Crawley, J.T.B. Crystal structure and substrate-induced activation of ADAMTS13. *Nat. Commun.* **2019**, *10*, 3781. [CrossRef]
26. Ercig, B.; Wichapong, K.; Reutelingsperger, C.P.M.; Vanhoorelbeke, K.; Voorberg, J.; Nicolaes, G.A.F. Insights into 3D Structure of ADAMTS13: A Stepping Stone towards Novel Therapeutic Treatment of Thrombotic Thrombocytopenic Purpura. *Thromb. Haemost.* **2018**, *118*, 28–41. [CrossRef]
27. Kim, H.J.; Xu, Y.; Petri, A.; Vanhoorelbeke, K.; Crawley, J.T.B.; Emsley, J. Crystal structure of ADAMTS13 CUB domains reveals their role in global latency. *Sci. Adv.* **2021**, *7*, eabg4403. [CrossRef]
28. South, K.; Luken, B.M.; Crawley, J.T.; Phillips, R.; Thomas, M.; Collins, R.F.; Deforche, L.; Vanhoorelbeke, K.; Lane, D.A. Conformational activation of ADAMTS13. *Proc. Natl. Acad. Sci. USA* **2014**, *111*, 18578–18583. [CrossRef]
29. Zanardelli, S.; Crawley, J.T.; Chion, C.K.; Lam, J.K.; Preston, R.J.; Lane, D.A. ADAMTS13 substrate recognition of von Willebrand factor A2 domain. *J. Biol. Chem.* **2006**, *281*, 1555–1563. [CrossRef]
30. Feys, H.B.; Pareyn, I.; Vancraenenbroeck, R.; De Maeyer, M.; Deckmyn, H.; Van Geet, C.; Vanhoorelbeke, K. Mutation of the H-bond acceptor S119 in the ADAMTS13 metalloprotease domain reduces secretion and substrate turnover in a patient with congenital thrombotic thrombocytopenic purpura. *Blood* **2009**, *114*, 4749–4752. [CrossRef]
31. Zhang, P.; Pan, W.; Rux, A.H.; Sachais, B.S.; Zheng, X.L. The cooperative activity between the carboxyl-terminal TSP1 repeats and the CUB domains of ADAMTS13 is crucial for recognition of von Willebrand factor under flow. *Blood* **2007**, *110*, 1887–1894. [CrossRef] [PubMed]
32. Ai, J.; Smith, P.; Wang, S.; Zhang, P.; Zheng, X.L. The proximal carboxyl-terminal domains of ADAMTS13 determine substrate specificity and are all required for cleavage of von Willebrand factor. *J. Biol. Chem.* **2005**, *280*, 29428–29434. [CrossRef] [PubMed]
33. Soejima, K.; Matsumoto, M.; Kokame, K.; Yagi, H.; Ishizashi, H.; Maeda, H.; Nozaki, C.; Miyata, T.; Fujimura, Y.; Nakagaki, T. ADAMTS-13 cysteine-rich/spacer domains are functionally essential for von Willebrand factor cleavage. *Blood* **2003**, *102*, 3232–3237. [CrossRef] [PubMed]
34. Porter, S.; Clark, I.M.; Kevorkian, L.; Edwards, D.R. The ADAMTS metalloproteinases. *Biochem. J.* **2005**, *386*, 15–27. [CrossRef] [PubMed]
35. Cerdà-Costa, N.; Xavier Gomis-Rüth, F. Architecture and function of metallopeptidase catalytic domains. *Protein Sci.* **2014**, *23*, 123–144. [CrossRef]
36. Nagase, H.; Visse, R.; Murphy, G. Structure and function of matrix metalloproteinases and TIMPs. *Cardiovasc. Res.* **2006**, *69*, 562–573. [CrossRef]

37. Hershko, K.; Simhadri, V.L.; Blaisdell, A.; Hunt, R.C.; Newell, J.; Tseng, S.C.; Hershko, A.Y.; Choi, J.W.; Sauna, Z.E.; Wu, A.; et al. Cyclosporin A impairs the secretion and activity of ADAMTS13 (a disintegrin and metalloprotease with thrombospondin type 1 repeat). *J. Biol. Chem.* **2012**, *287*, 44361–44371. [CrossRef]
38. Ricketts, L.M.; Dlugosz, M.; Luther, K.B.; Haltiwanger, R.S.; Majerus, E.M. O-fucosylation is required for ADAMTS13 secretion. *J. Biol. Chem.* **2007**, *282*, 17014–17023. [CrossRef]
39. Sorvillo, N.; Kaijen, P.H.; Matsumoto, M.; Fujimura, Y.; van der Zwaan, C.; Verbij, F.C.; Pos, W.; Fijnheer, R.; Voorberg, J.; Meijer, A.B. Identification of N-linked glycosylation and putative O-fucosylation, C-mannosylation sites in plasma derived ADAMTS13. *J. Thromb. Haemost.* **2014**, *12*, 670–679. [CrossRef]
40. Verbij, F.C.; Stokhuijzen, E.; Kaijen, P.H.P.; van Alphen, F.; Meijer, A.B.; Voorberg, J. Identification of glycans on plasma-derived ADAMTS13. *Blood* **2016**, *128*, e51–e58. [CrossRef]
41. Colige, A.C. Challenges and Solutions for Purification of ADAMTS Proteases: An Overview. *Methods Mol. Biol.* **2020**, *2043*, 45–53. [CrossRef] [PubMed]
42. Zheng, X.; Nishio, K.; Majerus, E.M.; Sadler, J.E. Cleavage of von Willebrand Factor Requires the Spacer Domain of the Metalloprotease ADAMTS13 *. *J. Biol. Chem.* **2003**, *278*, 30136–30141. [CrossRef] [PubMed]
43. Crawley, J.T.B.; Lam, J.K.; Rance, J.B.; Mollica, L.R.; O'Donnell, J.S.; Lane, D.A. Proteolytic inactivation of ADAMTS13 by thrombin and plasmin. *Blood* **2005**, *105*, 1085–1093. [CrossRef] [PubMed]
44. Kokame, K.; Nobe, Y.; Kokubo, Y.; Okayama, A.; Miyata, T. FRETS-VWF73, a first fluorogenic substrate for ADAMTS13 assay. *Br. J. Haematol.* **2005**, *129*, 93–100. [CrossRef]
45. Mackie, I.; Mancini, I.; Muia, J.; Kremer Hovinga, J.; Nair, S.; Machin, S.; Baker, R. International Council for Standardization in Haematology (ICSH) recommendations for laboratory measurement of ADAMTS13. *Int. J. Lab. Hematol.* **2020**, *42*, 685–696. [CrossRef]
46. George, J.N. Measuring ADAMTS13 activity in patients with suspected thrombotic thrombocytopenic purpura: When, how, and why? *Transfusion* **2015**, *55*, 11–13. [CrossRef]
47. Di Stasio, E.; Lancellotti, S.; Peyvandi, F.; Palla, R.; Mannucci, P.M.; De Cristofaro, R. Mechanistic Studies on ADAMTS13 Catalysis. *Biophys. J.* **2008**, *95*, 2450–2461. [CrossRef]
48. Yu, S.; Liu, W.; Fang, J.; Shi, X.; Wu, J.; Fang, Y.; Lin, J. AFM Imaging Reveals Multiple Conformational States of ADAMTS13. *J. Biol. Eng.* **2019**, *13*, 9. [CrossRef]
49. Hunt, R.; Hettiarachchi, G.; Katneni, U.; Hernandez, N.; Holcomb, D.; Kames, J.; Alnifaidy, R.; Lin, B.; Hamasaki-Katagiri, N.; Wesley, A.; et al. A Single Synonymous Variant (c.354G>A [p.P118P]) in ADAMTS13 Confers Enhanced Specific Activity. *Int. J. Mol. Sci.* **2019**, *20*, 5734. [CrossRef]
50. Cesco BelloCell. BelloCell-500 Technical Report VIII. Available online: https://chemglass.com/download/getmanual/1389 (accessed on 24 December 2021).
51. Soejima, K.; Nakamura, H.; Hirashima, M.; Morikawa, W.; Nozaki, C.; Nakagaki, T. Analysis on the Molecular Species and Concentration of Circulating ADAMTS13 in Blood. *J. Biochem.* **2006**, *139*, 147–154. [CrossRef]
52. Zou, G.; Kosikova, M.; Kim, S.R.; Kotian, S.; Wu, W.W.; Shen, R.; Powers, D.N.; Agarabi, C.; Xie, H.; Ju, T. Comprehensive analysis of N-glycans in IgG purified from ferrets with or without influenza A virus infection. *J. Biol. Chem.* **2018**, *293*, 19277–19289. [CrossRef] [PubMed]
53. Yang, S.; Wu, W.W.; Shen, R.; Sjogren, J.; Parsons, L.; Cipollo, J.F. Optimization of O-GIG for O-Glycopeptide Characterization with Sialic Acid Linkage Determination. *Anal. Chem.* **2020**, *92*, 10946–10951. [CrossRef] [PubMed]
54. Kaufman, R.J. Post-translational modifications required for coagulation factor secretion and function. *Thromb. Haemost.* **1998**, *79*, 1068–1079. [CrossRef] [PubMed]
55. Karlaftis, V.; Perera, S.; Monagle, P.; Ignjatovic, V. Importance of post-translational modifications on the function of key haemostatic proteins. *Blood Coagul Fibrinolysis* **2016**, *27*, 1–4. [CrossRef]
56. Wang, L.W.; Leonhard-Melief, C.; Haltiwanger, R.S.; Apte, S.S. Post-translational Modification of Thrombospondin Type-1 Repeats in ADAMTS-like 1/Punctin-1 by C-Mannosylation of Tryptophan*. *J. Biol. Chem.* **2009**, *284*, 30004–30015. [CrossRef]
57. Böhm, E.; Seyfried, B.K.; Dockal, M.; Graninger, M.; Hasslacher, M.; Neurath, M.; Konetschny, C.; Matthiessen, P.; Mitterer, A.; Scheiflinger, F. Differences in N-glycosylation of recombinant human coagulation factor VII derived from BHK, CHO, and HEK293 cells. *BMC Biotechnol.* **2015**, *15*, 87. [CrossRef]
58. Lind, T.; Birch, M.A.; McKie, N. Purification of an insect derived recombinant human ADAMTS-1 reveals novel gelatin (type I collagen) degrading activities. *Mol. Cell Biochem.* **2006**, *281*, 95–102. [CrossRef]
59. Balakirev, M.Y.; Mullally, J.E.; Favier, A.; Assard, N.; Sulpice, E.; Lindsey, D.F.; Rulina, A.V.; Gidrol, X.; Wilkinson, K.D. Wss1 metalloprotease partners with Cdc48/Doa1 in processing genotoxic SUMO conjugates. *eLife* **2015**, *4*, e06763. [CrossRef]
60. Imai, K.; Okada, Y. Purification of matrix metalloproteinases by column chromatography. *Nat. Protoc.* **2008**, *3*, 1111–1124. [CrossRef]
61. Ho, L.; Greene, C.L.; Schmidt, A.W.; Huang, L.H. Cultivation of HEK 293 cell line and production of a member of the superfamily of G-protein coupled receptors for drug discovery applications using a highly efficient novel bioreactor. *Cytotechnology* **2004**, *45*, 117–123. [CrossRef]
62. Waugh, D.S. An overview of enzymatic reagents for the removal of affinity tags. *Protein Expr. Purif.* **2011**, *80*, 283–293. [CrossRef] [PubMed]

63. Alexaki, A.; Hettiarachchi, G.K.; Athey, J.C.; Katneni, U.K.; Simhadri, V.; Hamasaki-Katagiri, N.; Nanavaty, P.; Lin, B.; Takeda, K.; Freedberg, D. Effects of codon optimization on coagulation factor IX translation and structure: Implications for protein and gene therapies. *Sci. Rep.* **2019**, *9*, 15449. [CrossRef] [PubMed]
64. Mauro, V.P.; Chappell, S.A. A critical analysis of codon optimization in human therapeutics. *Trends Mol. Med.* **2014**, *20*, 604–613. [CrossRef] [PubMed]
65. Jayapal, K.P.; Wlaschin, K.F.; Hu, W.; Yap, M.G. Recombinant protein therapeutics from CHO cells-20 years and counting. *Chem. Eng. Prog.* **2007**, *103*, 40.
66. Kim, J.Y.; Kim, Y.-G.; Lee, G.M. CHO cells in biotechnology for production of recombinant proteins: Current state and further potential. *Appl. Microbiol. Biotechnol.* **2012**, *93*, 917–930. [CrossRef]